

Chapter 2

PET Imaging Basics

Timothy G. Turkington

PET Radiotracers

Positron emission tomography (PET) imaging is the injection (or inhalation) of a substance containing a positron emitter, the subsequent detection of the emitted radiation by a scanner, and the computation of a digital image that represents the distribution of the radiotracer in the body.

Nuclide is the name for a specific combination of protons and neutrons that make up a nucleus, and a *radionuclide* is a nonstable nuclide, which will eventually decay. The most common nomenclature for nuclides is to specify the element name or symbol (which in turn specifies the number of protons) and the mass number, which is the sum of protons and neutrons. Typical ways to designate the nuclide with eight protons and eight neutrons are fluorine-18, ^{18}F , and $[\text{F}-18]$. Many radionuclides emit a positron upon decaying. The positron is a subatomic particle identical to the electron in some ways, but opposite in all the ways that particles can be opposite. It therefore has the same mass as an electron, but opposite charge. The symbol e^+ is used to represent the positron.

The time-dependence of the radioactive decay of a radionuclide is typically expressed as its half-life. The half-life is the time during which half of the substance decays. Such a parameterization is appropriate for an exponentially decaying process.

While many radionuclides decay via positron emission, only a few have been used much for PET imaging. The most commonly used are:

Nuclide	Half-life
C-11	20.3 min
N-13	10 min
O-15	124 s
F-18	110 min
Rb-82	75 s

T.G. Turkington (✉)
PET Facility, DUMC 3949, Durham, NC, 27710, USA
e-mail: timothy.turkington@duke.edu

The first four are produced by a particle accelerator (usually a cyclotron). For example, to produce fluorine-18, a beam of accelerated protons hits a target containing water with oxygen-18. From the interaction of a proton and oxygen-18 nucleus, a fluorine-18 nucleus and neutron are emitted.

Rubium-82 comes from the decay of strontium-82, which has a 25-day half-life. A generator containing strontium-82 can be used for approximately 1 month to provide rubidium-82 doses.

Coincidence Detection Physics

Positron Annihilation

After a positron is emitted, it travels a short distance (~ 1 mm) in tissue, losing energy by exciting and ionizing nearby atoms. Once it has lost almost all kinetic energy, it annihilates with a nearby electron. The product of this annihilation is a pair of photons. Conservation of energy and momentum dictate that the two photons depart in opposite directions, each with energy 511 keV.

Coincidence Detection

The emission of two photons from positron decay is shown in Fig. 2.1. Three possible trajectories are shown. Of all the possible trajectories, only a few, such as the ones shown, would be directed toward the depicted ring of detectors. One pair is shown making a signal in the corresponding detectors. The detectors consist of a scintillator, which converts energy from the 511-keV photon into many lower-energy light photons, and a photomultiplier, which converts the light into an electronic pulse. The creation of two electronic pulses at the same time (“in coincidence”) is a signal that there was an annihilation somewhere in the column or line of response (LOR) connecting the associated detectors. During the scan, coincidence counts are recorded for each LOR. The number of coincidence counts obtained on a particular LOR indicates

the amount of radioactivity present along that line during the scan. A parallel set of LORs then measures a projection of the radioactivity distribution, as illustrated in Fig. 2.2. This information is similar to what would be obtained with a collimated gamma camera at a particular angle. An important difference between PET and single photon imaging is that a gamma camera is measuring one projection at a time, whereas a PET camera is measuring all angles simultaneously.

Image Reconstruction

It is typical to store and display the raw data from a PET detector ring in a sinogram. In this format, the lines of response

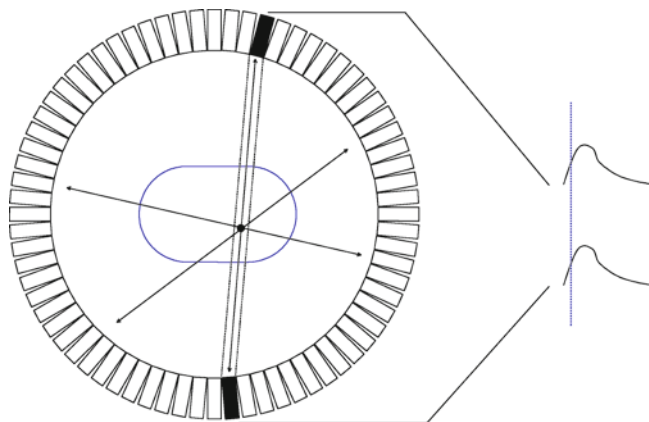


Fig. 2.1 Emission and detection of photons from annihilation point. Three possible trajectories are shown for a specific annihilation site. Many other trajectories are possible, the vast majority of which will not be in the plane of the detector ring. Two detectors indicate hits, and the system records a count for that line of response. The shaded area shows all possible locations from which the two photons could have originated and be detected in these two detectors

are sorted into parallel subsets, each of which represents a projection angle. Each subset (or angle) is represented by a row in an image. The image reconstruction process starts with raw data (sinograms) and produces cross-sectional images that represent that radioactivity distribution. Many algorithms have been proposed and used for this task. The images of Fig. 2.3 show the results of two popular algorithms for reconstructing PET images, filtered backprojection (FBP), and ordered subsets expectation maximization (OSEM), an iterative algorithm.

The images that result from PET provide quantitative information. After corrections (to be described) and image reconstruction, each image is a pixel-by-pixel representation of the radiotracer concentration at scan time. In some cases, scan protocols are performed to provide more physiologically

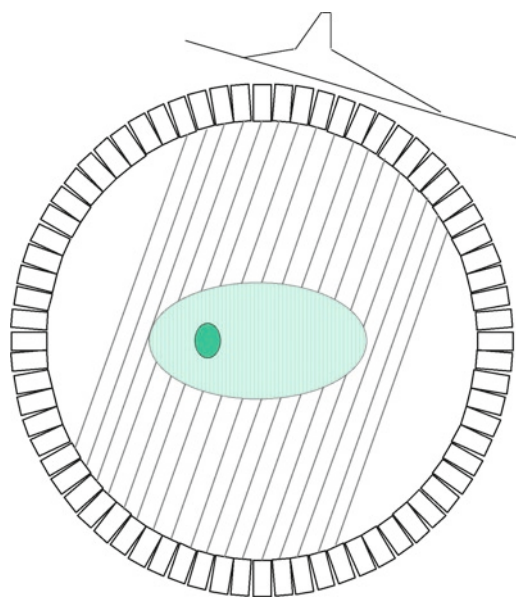
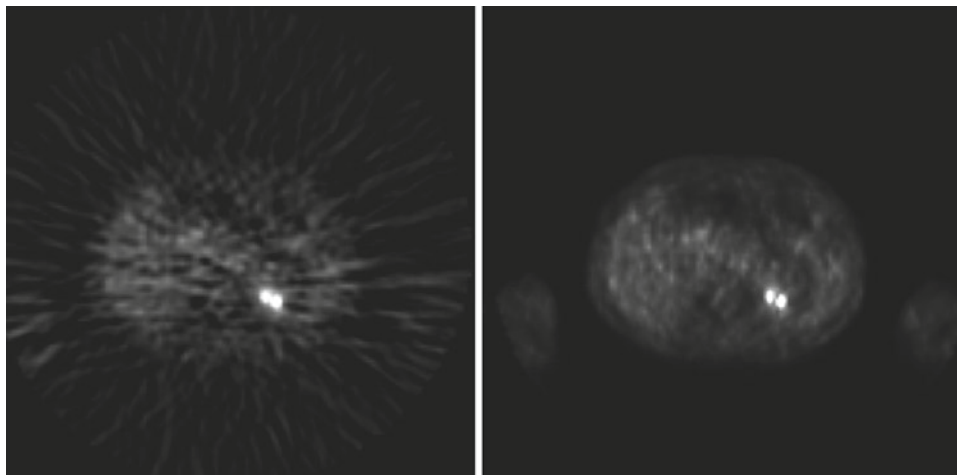


Fig. 2.2 Radioactivity measurement shown for a parallel set of lines of response, equivalent to a projection of the radioactivity distribution. There is a uniform background in the body with a single hot lesion

Fig. 2.3 Images reconstructed from the same raw data reconstructed with filtered backprojection (FBP) at left and ordered subsets expectation maximization (OSEM) at right. The most noticeable difference is the noise structure and the prevalence of noise at different activity levels. With FBP, the noise level is similar throughout the image. With OSEM, and other iterative algorithms, the noise levels are highest where the radioactivity levels are highest



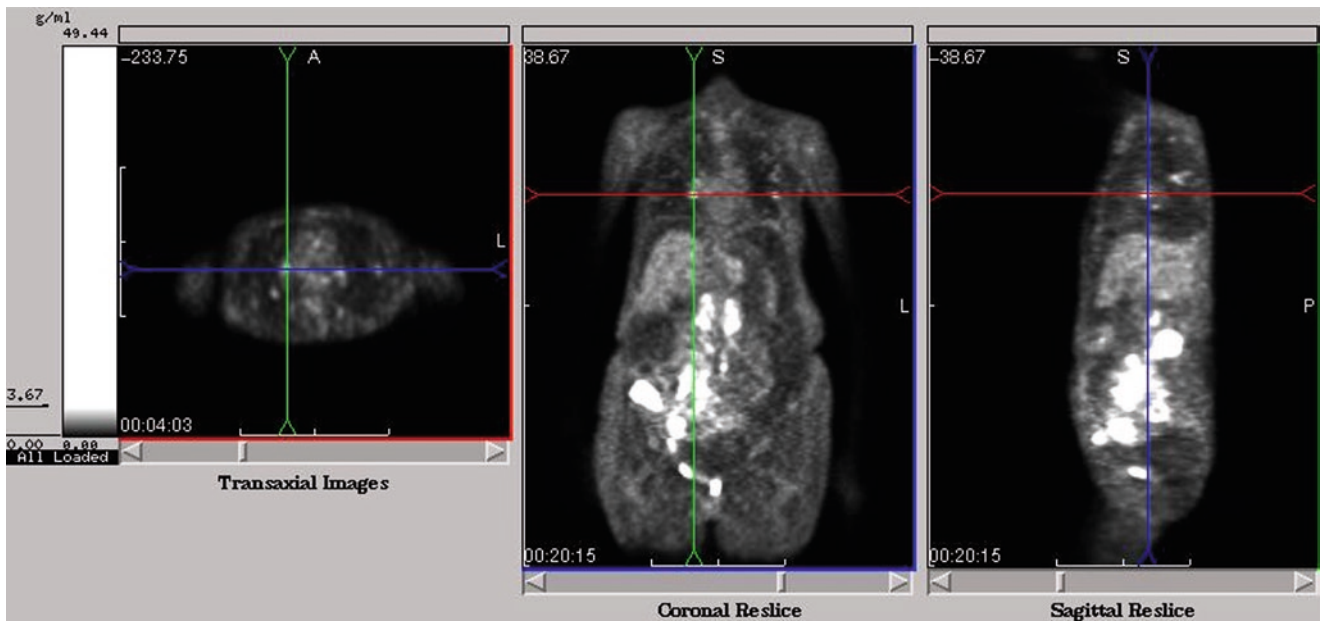


Fig. 2.4 Orthogonally reformatted images from a multi-slice PET acquisition

meaningful quantitation, such as glucose metabolic rate, or blood flow. In general, these require knowledge of the radiotracer concentration in the arterial blood, finely sampled, starting at injection time. Often, they also require the acquisition of dynamic data, that is, repeated scans starting at injection time that show the time course of radiotracer in the tissue of interest.

When multi-slice data are acquired and reconstructed (which is typical for all modern PET systems), it is possible to reformat the data into orthogonal planes, as shown in Fig. 2.4. Additional, oblique planes can be produced, as is typically done with cardiac PET and some brain protocols.

Background Events

Background events in PET imaging include the scattered event and the random event. The presence of these background events is detrimental to the quality of the resulting images.

Scattered Events

In a scattered event, one or both of the photons scatters in body tissue, changing direction and losing energy, but it is still detected. In Fig. 2.5 (left), two different possible trajectories for a scattered photon are shown. In each case, the resulting line of response does not contain the annihilation location. In one case, the line of response is entirely outside

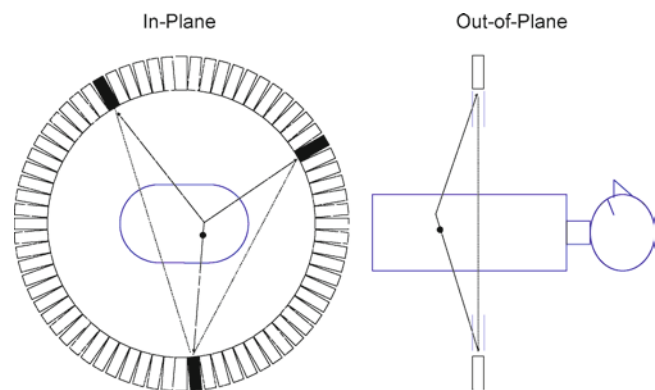


Fig. 2.5 At left two scatter possibilities for an emission photon pair. One leads to a coincidence appearing to come from within the body, and the other leads to a coincidence appearing to come from outside the body. At right is a side view depicting a different scattered event. This event appears to come from within the imaging plane, even though it does not. Shields placed in front and behind the detector ring (*dashed line*) would preclude such an event from being detected. On a multi-ring PET system, thin shields can be placed at each of the seams between rings to provide the same effect. In this case they are called septa

the body, which is a phenomenon unique to PET. (In single-photon emission or transmission modalities, scattered radiation always appears to come from the scattering medium.) In Fig. 2.5 (right), a side view of the detector ring is shown, along with a scattered event originating outside the detector ring. Such events add background due to radioactivity outside the field of view. In general, scattered events will have in-plane and out-of-plane components. To limit the number of events with substantial out-of-plane components, shielding can be used in front of and behind the detector ring. Such shields are called septa. In addition to reducing the number

of detected scattered events, the septa also reduce the number of events lost to detector dead time and the number of random events.

Random Events

A random event is depicted in Fig. 2.6. The two photons measured are from different annihilations. While it is possible to measure four photons simultaneously from simultaneous annihilations, the probability of all four photons leaving the body unscattered is quite small, and measuring only two photons as depicted in Fig. 2.6 is much more likely than measuring three or four.

The rate at which random coincidences will be measured between detectors A and B is given by

$$R_R = 2\tau R_A R_B, \quad (2.1)$$

were R_A and R_B are the rates at which detectors A and B are detecting photons, respectively, and 2τ is the size of the timing window. This timing window, analogous to the energy window used to discriminate between scattered and nonscattered photons, is set large enough to allow true events to be accepted, but small enough to exclude as many random events as possible. Imprecision in the timing of individual photons is a limit of the detection process, but varies for different detector materials.

Background Events and Count Statistics

Counts measured during a PET scan include true, scattered, and random events:

$$P = T + S + R, \quad (2.2)$$

where P , T , S , and R , are the prompt, true, scattered, and random events, respectively, “prompt” being the term for any in-time coincidence. Since it is desired to reconstruct images with T events only, an estimate of true events, T' , is obtained as follows:

$$T' = P - S' - R', \quad (2.3)$$

where S' and R' are estimates of the number of scattered events and random events. These estimates come from the scatter correction and random correction algorithms.

Even with accurate corrections for scattered and random events, there is an inherent detrimental effect of this background.

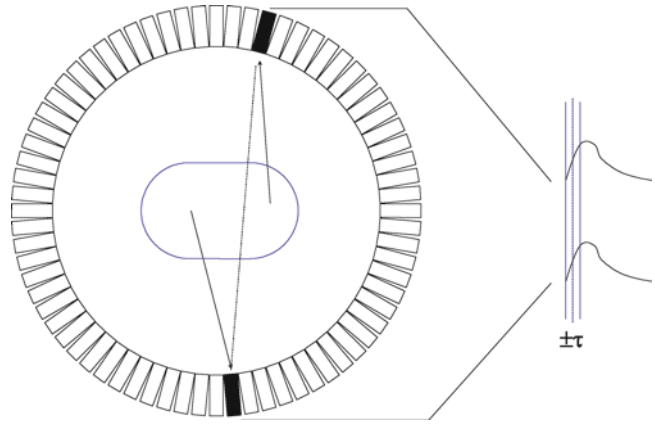


Fig. 2.6 A random event. Annihilation photons from two independent decays are emitted and detected at approximately the same time

The statistical quality of data with background present is inherently worse than that with no background present. For the T' calculated as above, the variance of T' is

$$\langle T' \rangle = \langle P \rangle + \langle S' \rangle + \langle R' \rangle, \quad (2.4)$$

where $\langle \rangle$ represents the variance on the enclosed quantity. That is, the variance of T is at least as large as the variance in the prompts measurement, which is dictated by Poisson statistics, and this is worse than the variance on T if there were no background at all.

The noise equivalent count (NEC) parameter has been developed to provide an estimate of image signal to noise ratio as a function of T , S , and R . A simplified version is

$$NEC = \frac{T}{(1 + \frac{S}{T} + \frac{R}{T})}. \quad (2.5)$$

This could refer to the statistical quality of data on a specific line of response, or the image quality resulting from all lines of response. In the latter case, background is only considered for lines of response that are within the imaged object. This particular formulation assumes noiseless scatter and random corrections. If the corrections are themselves noisy (such as the delayed event correction for random events), then the terms in the denominator are even larger. With no background, $NEC = T$. As background increases, NEC decreases for a fixed number of trued events.

Extended Axial Field of View and 3D PET

To obtain as many true counts as possible, PET systems incorporate multiple rings of detectors. While this would be of little or no benefit for imaging a single slice of the body,

the typical task of whole body imaging can be done with more time spent on each body section if the scanner's axial field of view is greater (assuming a fixed total time is allowed for the whole body scan). Available systems have 18–52 rings of detectors, providing a total axial field of view of at least 15 cm and up to almost 22 cm.

In multi-ring 2D PET, the septa are positioned at the seam between each crystal ring. Coincidences are recorded for photons detected within the same ring (direct planes), and for photons detected in adjacent rings (cross-planes).

In 3D PET, events are recorded regardless of which rings the two photons hit. Since the septa themselves limit the axial acceptance angle, they must be removed for all possible photon trajectories to actually be detected. Compared to the 2D mode of acquisition, 3D PET increases the system sensitivity for true events (approximately fivefold, but varying depending on the specifics of the septa and other factors). The fraction of events that are background rises dramatically, though as well, since septa are not present to limit scattered and random events. In addition, for a specific amount of radiation leaving the body, the individual detectors are much more likely to be hit without septa, and therefore dead-time issues are greater in 3D PET if the injected dose is kept constant.

The clearest benefit of 3D PET is in imaging the brain, where the scatter and random fractions are relatively low. In some applications, a lower injected dose must be used than could have been used in 2D, because of excessive losses due to dead time and the statistical effects of the random events.

The desire to benefit from the increased sensitivity of 3D PET has driven the development of improved radiation detectors. Good energy resolution is one desired trait, since photons lose energy when Compton scattering. The better a detector's energy resolution, the better it can reject scattered photons. Better timing resolution is another desired characteristic. The more precisely the photons' arrival time can be measured, the smaller the timing window can be used, rejecting more random events while retaining true events. Faster scintillators also decrease the number of events lost to dead time.

Revisiting the NEC formula (2.5), 3D imaging has the following direct effects

Increase in T (demonstrated by increased system sensitivity):	+NEC
Increase in S/T (depending on body size and radioactivity distribution):	–NEC
Increase in R/T :	–NEC

In addition, there are indirect effects. For example, the injected dose may need to be lower for 3D, due to count-rate and random event considerations, directly detracting from the increase in T . The degree to which 3D scanning

improves final image quality (if at all) depends on a variety of factors.

The currently available PET systems all achieve good image quality through different designs that capitalize on the properties of the detectors being used.

Spatial Resolution and Block Detectors

The spatial resolution of PET images is determined by several factors. Fundamental limits include the positron range (the scanner sees the annihilation location, not the emission location, which is of interest) and photon noncolinearity (the annihilation photon departure trajectories are not exactly 180° apart). Fortunately, these effects are relatively small.

An effect that can be controlled is the size of the detector. If events are always assigned to the correct detector (which is not always the case), smaller detectors yield improved spatial resolution. Several factors have limited the miniaturization of PET detector crystals. An important factor is that it is not feasible to couple each crystal to its own photomultiplier tube, if the crystals are small and numerous. A popular solution is to couple a matrix of crystals (6×6 , 8×8 , and up to 13×13) to a small number of photomultiplier tubes (four conventional tubes, or two tubes, each with two separate photosensitive regions, or a single tube with four independent quadrants). The relative pulse heights from the four photomultiplier signals are used to determine which crystal in the matrix was actually hit. This scheme leads to a large reduction in the required number of photomultipliers. For example, four photomultipliers on an 8×8 crystal matrix is one photomultiplier per 16 crystals. Using such a scheme, a PET system can have 10,000–20,000 crystals, each 4–6 mm in size, with only 1,000 photomultipliers. The reduction is even greater if a single, four-quadrant photomultiplier is used per block.

Attenuation

Attenuation is the loss of coincidence events through scatter or absorption of one or both of the annihilation photons in the body. While the photon energy is higher in PET than that of any single-photon emission radionuclide and the linear attenuation coefficient is relatively low, the requirement of detecting both photons yields a higher overall event-per-event attenuation probability. Fig. 2.7 depicts the quantitative attenuation considerations for coincidence imaging. Fig. 2.8 shows the probability of events surviving attenuation from a uniform distribution in a range of circular cylinder radii for both PET and 140 keV single photons. For objects the size of a head,

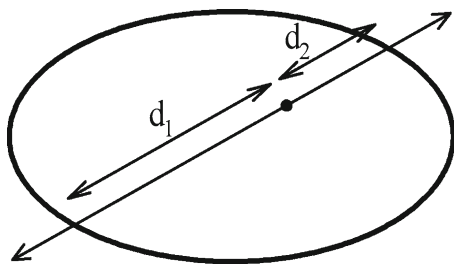


Fig. 2.7 Attenuation effects in PET. Each photon has an attenuation probability (shown for the uniform attenuation case), and the overall probability of both photons surviving is the product of the two. The result is that the overall probability for a specific line of response depends only on the summed trajectories of the two photons, independent of specific location on that line. (From Turkington TG, Attenuation correction in hybrid positron emission tomography. *Semin Nucl Med* 2000;30:255–267, with permission from Elsevier)

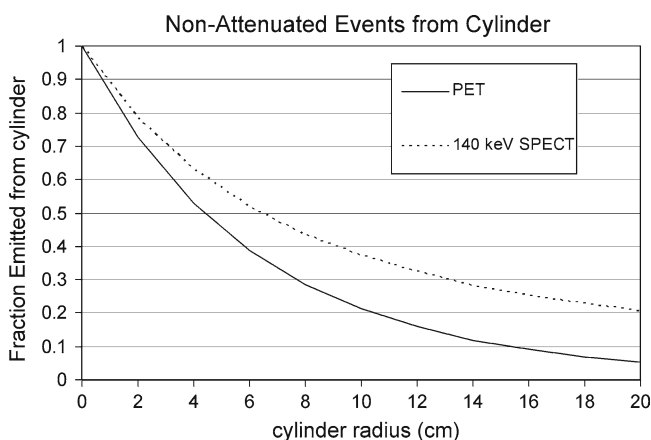


Fig. 2.8 Attenuation effects with increasing object size. For a uniform distribution of radioactivity in a circular cylinder of increasing radii, the probability of the event not being attenuated is shown for PET and for SPECT at 511 keV. (From Turkington TG, Attenuation correction in hybrid positron emission tomography. *Semin Nucl Med* 2000;30:255–267, with permission from Elsevier)

approximately 25% of photon pairs survive. For a small abdomen, approximately 10% survive. For a very large abdomen, the number surviving is not shown, but can be 1% or smaller.

This loss of events has several implications. First, image quality is degraded because of the decreased counts obtained from large body regions. This effect cannot be corrected. It can only be offset by using a higher injected dose (this is only possible if the scanner can accommodate the increased event rate; the individual detector rates do not decrease with size as quickly as coincidence rates), or a longer scan time. Given the wide range in attenuation differences between very large and very small patients (~10×) it would be very difficult to implement scan time variations of this magnitude in a busy setting. It is important to note that attenuation levels are independent of scanner design or operating parameters. However, attenuation effects are compounded by the effect of increased scatter fraction that occurs with larger bodies, as

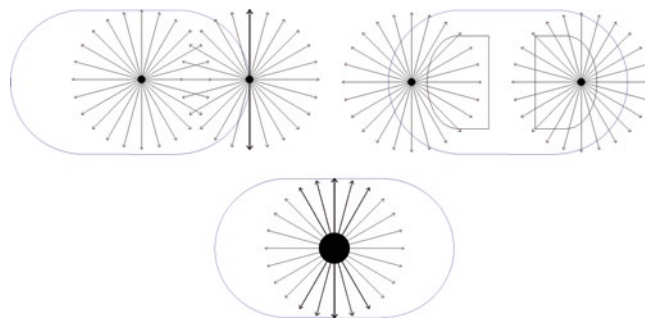


Fig. 2.9 Explanation of attenuation artifacts. *Upper left* depicts the tendency for radiation originating deeper in the body to suffer more attenuation, thereby appearing to have less uptake. The outer contour of the body is an extreme case, in which a narrow band of trajectories has no attenuation at all for either photon. The *upper right* depicts the effect of the lungs. Radiation originating in the lungs, or any other low-density area, will suffer less attenuation, even less than radiation from less-deep structures. At *bottom* is the effect typically seen with the bladder. Radiation emitted in the anterior-posterior direction is much more likely to be detected than radiation emitted in the lateral direction. The resulting reconstructed images show an elongation of the bladder in the direction of low attenuation, and depleted areas on the sides. This phenomenon would be true of any hot object with highly nonisotropic attenuation

well, and its additional effect on count statistics, as reflected in NEC.

Another implication of attenuation is the loss of quantitation in measurement of radioactivity concentration and other quantities derived from it. Tenfold or greater errors not only need to be corrected, but the correction must also be very accurate if any quantitative use is to be made.

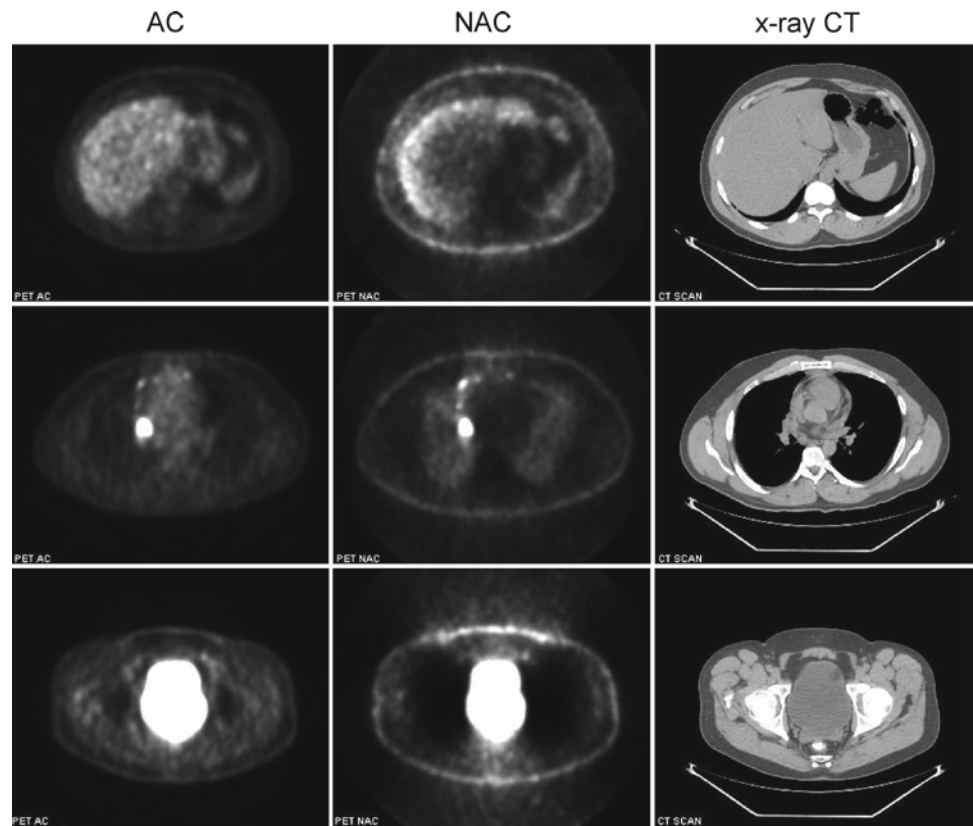
An additional factor with attenuation is the introduction of image artifacts; that is, features that make the image qualitatively unrepresentative of the actual radioactivity distribution. Three general types of PET attenuation artifacts are explained in Fig. 2.9 and depicted in Fig. 2.10.

Attenuation Correction

While the statistical effect of lost counts and the resulting image noise cannot be compensated, quantitative accuracy can be restored and attenuation-related artifacts can be removed with attenuation correction. Attenuation correction generally means taking into account the attenuation factor for each line of response; that is, the probability that photons emitted along each line of response will survive. The reciprocal of this factor, the attenuation correction factor, can be applied for each line of response, resulting in an estimate of the number of counts that would have been attained on each LOR.

If the outer contour of the body is known, and if all of the tissue within that boundary is of uniform density, then the

Fig. 2.10 Attenuation artifacts in PET. The three columns are attenuation-corrected PET (*left*), non-attenuation-corrected PET (*middle*), and x-ray CT (*right*) for anatomical reference. Notable artifacts in the non-corrected PET are the non-uniformity of the liver (*upper image*), the bright outer contour (all images), the apparent high activity in the lungs (*middle image*), the false high and low activity areas around the bladder (*lower image*). An additional effect is that concave areas in the body surface are not concave in the noncorrected image. That is, radioactivity shows up falsely in regions that were actually air. This phenomenon occurs internally, as well, for example in the top image a gaseous region adjacent to the liver shows activity falsely in the noncorrected image that is fixed by the attenuation correction



attenuation factor for each LOR can be calculated using the simple attenuation formula $e^{-\mu d}$, and the corresponding correction factor calculated and applied. These criteria are never strictly met in any section of the body, because of bone and lung, but it is common to use calculated attenuation correction for brain imaging if quantitation is not being used.

More accurate attenuation correction can be obtained with a transmission scan. A conventional scheme for PET transmission scanning uses one or more Ge-68 rods that orbit around the body, inside the detector ring for 1–5 min per bed position (Fig. 2.11). Ge-68 is a positron emitter, and therefore produces 511 keV photon pairs. The rod is as long as the axial field of view of the system. A transmission coincidence is measured similarly to an emission coincidence. Attenuation factors for each line of response are determined by dividing the counts obtained during a transmission scan by the counts obtained during a blank scan, which is a transmission scan performed with an empty gantry. Such radionuclide-based transmission scans have the benefits of using the same detectors as are used for emission events, and of having high accuracy, since the attenuation factors are determined with the same photon energy as is being corrected. The fundamental limit is that of statistics. There is a limit in the measurable transmission count rate, because of the PET detectors' limits (and exacerbated by the proximity of the source to the nearby detector ring). For a reasonable scan time (preferably shorter than the emission scan, since that

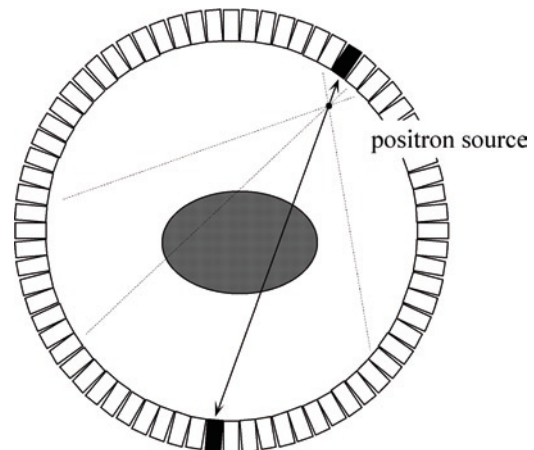


Fig. 2.11 Transmission scan geometry using a Ge-68 radionuclide source. The source orbits around the body, illuminating all possible lines of response, and by comparison with a blank scan, yielding the attenuation factors for each line

provides the fundamental information), the limited number of counts translates into additional noise in the corrected emission image.

A third option for attenuation correction is to use x-ray CT as the transmission data. Much short scans provide much lower-noise corrections. The use of x-ray CT for PET attenuation correction and the other considerations for combined PET-CT scanners are discussed in a later chapter.

PET Quantitation

Quantitative use of PET data requires accurate corrections for attenuation, scatter, random events, and dead time. The first step in quantitation is producing images whose pixel values represent the radioactivity concentration of the imaged object. In addition to the various corrections, calibration factors must be determined to translate the corrected counts to radioactivity values.

PET can be used to measure physiologic parameters, such as blood flow, or glucose metabolic rate, quantitatively. Quantitative measurements such as these require knowledge of the arterial blood radioactivity concentration as a function of time, starting at the injection, and can require multiple time points to be imaged (dynamic scanning).

Short of quantitating physiological parameters, the SUV (standardized uptake value) is an index that normalizes for the injected dose and body size in a simple way. The SUV is calculated as

$$SUV = \frac{\text{Radioactivity concentration}}{(\text{Injected dose})/(\text{Body mass})}. \quad (2.6)$$

Dividing by the injected dose normalizes the measured concentration to yield a dose-independent index. Multiplying by body mass (or dividing by it in the denominator) normalizes for the effect that a larger body has more competing tissue than a small body, compared to a given size tissue of interest. An alternate perspective is that the SUV is the concentration of tracer measured in a region, divided by the average concentration throughout the body. Since some of the tracer will typically have been voided by the time of the scan, this is not exactly correct, and an SUV of 1 will therefore be higher than the body average. Individual pixels can be calculated as SUV values, and regions-of-interest statistics (typically maximum and mean) can be reported in SUV.

References

1. Cherry SR, Sorenson JA, Phelps ME. Physics in Nuclear Medicine, 3rd edn. Philadelphia: Saunders, 2003.
2. Townsend DR, Bendriem B. The Theory and Practice of 3D PET. Dordrecht: Kluwer, 1998.
3. Turkington TG. Introduction to PET instrumentation. J Nucl Med Technol 2001;29:4-11.
4. Wernick MW, Aarsvold JN. Emission Tomography: the Fundamentals of PET and SPECT. San Diego: Elsevier, 2004.

Clinical PET-CT in Radiology

Integrated Imaging in Oncology

Shreve, P.; Townsend, D.W. (Eds.)

2011, XIV, 437 p. 690 illus., 149 illus. in color.,

Hardcover

ISBN: 978-0-387-48900-1